npj | Quantum Materials

www.nature.com/npjquantmats

ARTICLE OPEN

Check for updates

Nematicity in a cuprate superconductor revealed by angle-resolved photoemission spectroscopy under uniaxial strain

S. Nakata[1]✉, M. Horio[1], K. Koshiishi[1], K. Hagiwara[1], C. Lin[1], M. Suzuki[1], S. Ideta[2], K. Tanaka[2], D. Song[3], Y. Yoshida[3], H. Eisaki[3] and A. Fujimori[1,4]

The nature of the pseudogap and its relationship with superconductivity are one of the central issues of cuprate superconductors. Recently, a possible scenario has been proposed that the pseudogap state is a distinct phase characterized by spontaneous rotational symmetry breaking called "nematicity" based on transport and magnetic susceptibility measurements, where the symmetry breaking was observed below the pseudogap temperature T^*. Here, we report a temperature-dependent ARPES study of nematicity in slightly overdoped $Bi_{1.7}Pb_{0.5}Sr_{1.9}CaCu_2O_{8+\delta}$ triggered by a uniaxial strain applied along one of the Cu–O bond directions. While the nematicity was enhanced in the pseudogap state as in the previous studies, it was suppressed in the superconducting state. These results indicate that the pseudogap state is characterized by spontaneous rotational symmetry breaking and that the nematicity may compete with superconductivity. Relationship between the nematicity and charge-density waves, both of which are observed in the pseudogap state, is discussed.

npj Quantum Materials (2021)6:86 ; https://doi.org/10.1038/s41535-021-00390-x

INTRODUCTION

The pseudogap in cuprate superconductors is characterized by the suppression of the density of states around the Fermi level below a characteristic temperature T^* and above the superconducting transition temperature T_c. Broadly speaking, two possible scenarios for the pseudogap have been discussed, that is, a precursor to the superconducting state and distinct order which competes with superconductivity[1]. The latter scenario has been put forward by several measurements, which detect distinct orders with spontaneous symmetry breaking such as translational and time-reversal symmetry breaking at or below the pseudogap temperature T^*[2–17].

Recently, electronic nematicity that the electronic structure preserves the translational symmetry but breaks the rotational symmetry of the underlying crystal lattice has been found to exist in the pseudogap state[11–15,18,19]. As a possible mechanism, it has been proposed that the nematicity arises from fluctuations of stripe order[20,21] or from the instability of the Fermi surface (so-called Pomeranchuk instability)[22–26]. From experimental perspectives, the nematicity in the cuprate superconductors was first pointed out by transport measurements of lightly-doped $La_{2-x}Sr_xCuO_4$ and $YBa_2Cu_3O_y$ (YBCO)[11]. Anisotropic signals in the spin excitation measured by neutron scattering were observed for untwinned underdoped YBCO[12]. Inequivalent electronic states associated with the oxygen atoms in the *a* and *b* directions was detected by scanning tunneling spectroscopy measurements of underdoped $Bi_2Sr_2CaCu_2O_{8+\delta}$ (Bi2212)[14]. Circular dichroism in angle-resolved photoemission spectroscopy (ARPES) measurements of Bi2212 showed small differences between the (π, 0) and (0, π) regions, which was attributed to possible rotational symmetry breaking[16]. Nematic fluctuations in Bi2212 have been observed by Raman scattering[27]. Nernst effect and magnetic torque measurements on underdoped and optimally doped YBCO showed a systematic temperature dependence of the nematicity[13,15]. The onset temperature of the in-plane anisotropic signals in the Nernst coefficient and that in the magnetic susceptibility coincide with T^*. Furthermore the nematic susceptibility derived from elastoresistance experiments on Bi2212 diverges towards T^*[28]. The order parameter-like behaviors of the nematicity in the Nernst and magnetic torque experiments[13,15] and the divergence of the nematic susceptibility[28] indicate that the pseudogap state can be considered as a distinct thermodynamic phase characterized by the rotational symmetry breaking. Although the orthorhombic distortion of the CuO_2 plane caused by the Cu–O chains along the *b*-axis of the untwinned YBCO samples already breaks the four-fold rotational symmetry even above T^*, the orthorhombicity is considered to help the distortion of the electronic states of the CuO_2 plane in one particular direction and enables us to detect nematicity in macroscopic measurements. This weak orthorhombicity of the CuO_2 plane for nematicity plays the same role as a weak external magnetic field for ferromagnets[29].

Motivated by those previous studies on nematicity in the cuprates, we have performed ARPES measurements on slightly overdoped $Bi_{1.7}Pb_{0.5}Sr_{1.9}CaCu_2O_{8+\delta}$ (Pb-Bi2212) ($T_c = 91$ K) by applying a uniaxial strain along the Cu–O bond direction to detect nematicity below T^*. At the doping level we chose, T^* was not too high for ARPES experiments but the divergence of the nematic susceptibility in Pb-Bi2212 was sufficiently strong[28]. While most of the studies on nematicity in the cuprate superconductors have been done on YBCO, Pb-Bi2212, whose CuO_2 plane has the tetragonal (C_4) symmetry, is a more convenient material to study nematicity than YBCO. Owing to the presence of a natural cleavage plane between the BiO layers and rich information accumulated from previous ARPES studies, Bi2212 is an ideal

[1]Department of Physics, University of Tokyo, Bunkyo-ku, Tokyo 113-0033, Japan. [2]UVSOR Facility, Institute for Molecular Science, Okazaki 444-8585, Japan. [3]National Institute of Advanced Science and Technology (AIST), Tsukuba 305-8568, Japan. [4]Department of Applied Physics, Waseda University, Shinjuku-ku, Tokyo 169-8555, Japan. ✉email: s.nakata@fkf.mpg.de

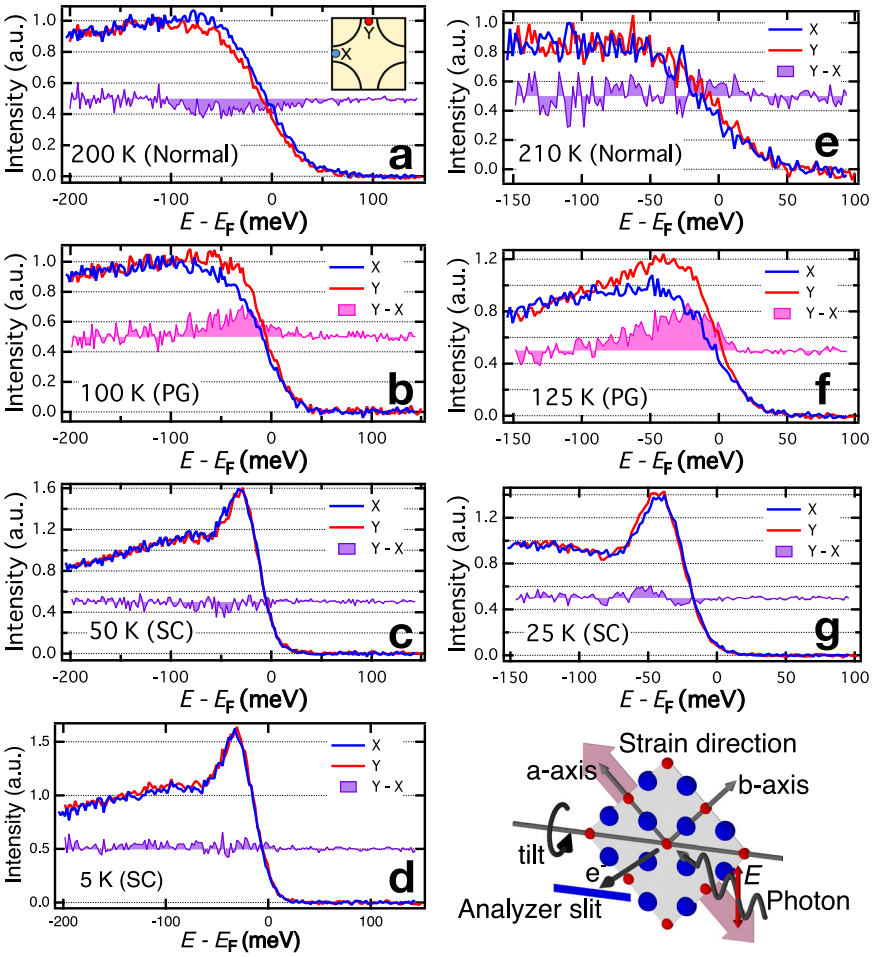

Fig. 1 Energy distribution curves (EDCs) of Pb-Bi2212 at various temperatures. The measurements were performed with decreasing temperature for **a**–**d** and increasing temperature for **e**–**g**. At each temperature, EDCs at the *X* and *Y* points and the difference between them are displayed. At each temperature, the spectra have been normalized at high energy in the displayed energy range. In the pseudogap state ($T = 100$ and 125 K), the spectral intensities between the *X* and *Y* points are clearly different while they are nearly identical in the normal ($T =$ 200 and 210 K) and superconducting states ($T = 5$, 25, and 50 K). Inset shows the experimental geometry including the crystallographic axes, the strain direction, light polarization, and the analyzer slit, which ensure the spectroscopic equivalence of the *a*-axis and *b*-axis directions.

material for ARPES experiment to investigate novel phenomena in cuprates[30]. In the present work, we analyze the single particle spectra without assuming that the symmetry of the electronic structure is the same as the symmetry of the CuO_2 plane, in order to shed light on the possibly lowered symmetry of the electronic structure. Furthermore, using ARPES, one can investigate the nematicity not only in the normal and pseudogap states but also in the superconducting state, where transport and magnetic measurements cannot be used due to the zero resistivity and the strong diamagnetism, respectively[13,15,18].

RESULTS

Energy distribution curves

In Fig. 1, energy distribution curves (EDCs) around $\boldsymbol{k} = (-\pi, 0)$ (*X* point) and $(0, \pi)$ (*Y* point) at various temperatures are shown. The data were obtained from one sample but from two cleavages: on one cleaved surface, we performed ARPES measurements with cooling the sample at $T = 5$, 50, 100, and 200 K and, on the other cleaved surface, with heating the sample at $T = 25$, 125, and 210 K. In both measurements, the tensile strain was applied in the *x*-direction (||*a*-axis) as shown in the inset of Fig. 1. In the cooling series, $T = 200\ \text{K} \rightarrow 100\ \text{K} \rightarrow 50\ \text{K} \rightarrow 5\ \text{K}$, in the normal state (200 K), the line shapes of the EDCs were almost identical between the *X* and *Y* points, as expected from the four-fold rotational symmetry of the CuO_2 plane. With decreasing temperature, the line shapes of the EDCs around the *X* and *Y* points became different below T^* in the pseudogap state (100 K) and then nearly identical again below T_c in the superconducting state (5 and 50 K). In the heating series, $T = 25\ \text{K} \rightarrow 125\ \text{K} \rightarrow 210\ \text{K}$, the spectral changes of the cooling series was reproduced as shown in Fig. 1. Let us focus on the pseudogap state, where difference in the line shapes of the EDCs is present between the *X* and *Y* points. In Bi2212, it is well known that the Cu–O band is split into the anti-bonding and bonding bands due to the bilayer structure[31]. From the dispersions near $\boldsymbol{k} = (\pi, 0)$ in overdoped sample ($T_c = 91$ K), whose doping level is the same as the present sample, we consider that the energies of the bottoms of the anti-bonding band and bonding band are located around $E - E_F = -25$ meV and -110 meV, respectively, in the pseudogap state. (See Supplementary Note 1) Thus, we conclude that the intensity of the bonding (anti-bonding) band is higher around the *X* (*Y*) point than that around the *Y* (*X*) point, reflecting the in-plane anisotropy of the electronic structure in the pseudogap state under the uniaxial strain. Here, we would like to emphasize that this inequivalence between the *X* and *Y* points is caused by the lowered symmetry of the initial state and hence of the matrix elements because the *x*-directions and *y*-directions are equivalent for a tetragonal sample in the present measurement geometry (See also Supplementary Note 2). The

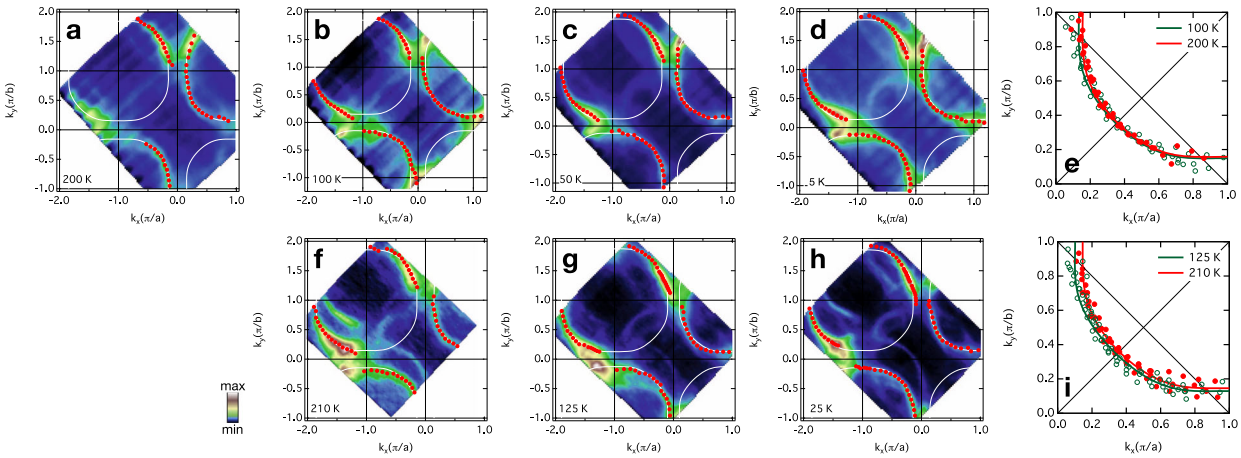

Fig. 2 Constant-energy-surface mapping of the ARPES spectra of Pb-Bi2212 taken at various temperatures. The measurements were performed with decreasing temperature (**a**–**d**) and increasing temperature (**f**–**h**). The constant energy is $E - E_F = -25$ meV (**a**–**d**) and -20 meV (**f**–**h**) and the intensity is integrated within ±10 meV of the constant energy. Red circles show the constant-energy surface determined from the peaks of the momentum distribution curves (MDCs). White curves are the fitted curves using the tight-binding model of Eq. (2). **e** Constant-energy surface at 100 and 200 K folded in the first quadrant of the first Brillouin zone and fitted curves in a range allowed by the symmetry. **i** Same as **e** but the data at 125 and 210 K.

modification of the matrix elements due to the lowered initial-state symmetry plausibly explains, why the EDCs at the higher energy scale than the pseudogap itself were affected.

Constant energy surfaces

In Fig. 2, the intensity maps of the constant-energy surface at $E - E_F = -25$ meV (**a**–**d**) and -20 meV (**f**–**h**) at various temperatures are displayed. We have analyzed the constant-energy surface rather than the Fermi surface because the dispersion of quasiparticles near E_F is partially gapped due to the pseudogap and superconducting gap opening at low temperatures. The intensity around $k_y = -k_x$ almost vanishes due to matrix-element effect (See Supplementary Note 3 for the matrix-element effect). The diffraction replica due to the modulation in the Bi–O layer is completely suppressed in the Pb-doped sample while the well-known diffraction replica shifted by (π, π) was still observed. (See Supplementary Note 4 and 5) At $\boldsymbol{k} = (\pi, 0)$ for $h\nu = 60$ eV, the intensity of the anti-bonding band is only a little weaker than the bonding band but not negligible[32,33], and their MDC widths are large (~ 0.3 π/a FWHM) compared to the momentum separation of the two bands (~0.2 π/a). (See Supplementary Note 2) Therefore, we extracted the constant-energy surface practically as a single band rather than multiple bands, i.e., overlapping anti-bonding and bonding bands. The constant-energy surface has been determined from the peak positions of the MDCs fitted using Lorentzians. In Fig. 2e, i, the constant-energy surface in the pseudogap state and the normal state folded in the first quadrant of the first Brillouin zone are overlaid on each other and compared. The constant-energy surface around the Y point in the pseudogap state is closer to $(0, \pi)$ than that in the normal state. This is consistent with the observation displayed in Fig. 1b, f that the intensity of the anti-bonding (bonding) band becomes stronger near the Y (X) point in the pseudogap state. Therefore, we interpret the intensity transfer from the bonding band to anti-bonding band as one goes from the X point to the Y point shown in Fig. 1b, f distort the constant-energy surface around the Y point.

To understand the anisotropy of the constant-energy surface more quantitatively, we have estimated it with the tight-binding model in the following way. Because we ignore the splitting of the constant-energy surface as described above, constant-energy surfaces near the Fermi level can be fitted using single-band tight-binding model

$$\varepsilon(k_x, k_y) - \mu = \varepsilon_0 - 2t(\cos k_x + \cos k_y) - 4t'\cos k_x \cos k_y - 2t''(\cos 2k_x + \cos 2k_y), \quad (1)$$

where t, t', and t'' are the nearest-neighbor, second-nearest-neighbor, and third-nearest-neighbor hopping parameters, respectively, and μ is the chemical potential[34]. The model has four-fold rotational (C_4) symmetry. In order to examine the possibility of the C_4 rotational symmetry breaking into C_2 symmetry, we introduce an anisotropy parameter δ which represents the orthorhombicity of the hopping parameters (t and t'')[23] as

$$\varepsilon(k_x, k_y) - \mu = \varepsilon_0 - 2t[(1-\delta)\cos k_x + (1+\delta)\cos k_y] - 4t'\cos k_x \cos k_y - 2t''[(1-\delta)\cos 2k_x + (1+\delta)\cos 2k_y]. \quad (2)$$

By fitting the constant-energy surface using Eq. (2), we have estimated its deviation from the C_4 symmetry through the finite δ values (For detailed fitting procedures, see Supplementary Note 6).

The temperature dependence of the anisotropy parameter δ thus derived is shown in Fig. 3. In the normal state ($T > T^*$), δ is close to zero, in both heating and cooling series, which was expected from the four-fold rotational symmetry of the CuO_2 plane. It is also consistent with the EDCs in Fig. 1a, e. In the

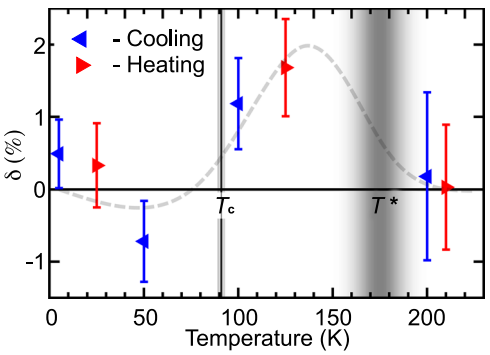

Fig. 3 Temperature dependence of the anisotropy parameter δ. δ is defined by Eq. (2). The values have been determined by fitting Eq. (2) to the constant-energy-surface mappings in Fig. 2. The error bars are standard errors of the fitting parameter at each temperature. The dashed gray line is a guide to the eye.

pseudogap state ($T_c < T < T^*$), however, δ became finite. The sign of δ indicates that the hopping parameters along the tensile strain direction became small in the pseudogap state. The sign of δ is also the same as the anisotropic Fermi surface of $YBa_2Cu_4O_8$ under the uniaxial strain from the Cu–O chains leading to the small difference between the a and b lattice constants[35]. Thus, the uniaxial strain seems to serve as an external perturbation to align a majority of nematic domains in one direction (See also Supplementary Note 7 for the effect of strain on the magnitude of the hopping parameters). Figure 3 also shows that δ is suppressed in the superconducting state. In the normal and pseudogap states, our result is consistent with the previous magnetic and transport measurements on YBCO in that the nematicity becomes finite below T^*[13,15]. More concretely, for example, the anisotropy of the magnetic susceptibility of YBCO, which was derived from the magnetic torque measurements[13] is as large as 0.5% just above T_c. Although further studies are necessary to compare the magnetic susceptibility and the single-particle spectral function quantitatively, we naively believe that the δ whose order of magnitude was 1% in our measurements would have high impacts on various physical properties such as charge and magnetic susceptibilities. As for the superconducting state, the magnetic and transport measurements cannot give any information about the possible symmetry breaking, because of the giant diamagnetism and zero resistivity, respectively, while our ARPES result indicates possible competition between nematicity and superconductivity.

DISCUSSION

From the theoretical side, dynamical mean-field theory (DMFT) combined with the fluctuation exchange (FLEX) approximation for the Hubbard model has shown that a Pomeranchuk instability, where the C_2 anisotropy of the Fermi surface is induced, appears in the overdoped region but coexists with superconductivity[34]. In contrast, according to a cellular dynamical mean-field theory (CDMFT) study for the Hubbard model, the C_4 symmetry breaking was shown in the underdoped pseudogap regime rather than in the overdoped regime[36,37]. According to mean-field calculations of the $t-J$ model, the Pomerachuk instability competes with superconductivity[22,38]. Thus, it is not clear at present whether the Pomeranchuk instability consistently explains our result or not.

Nematicity has also been considered as arising from fluctuations of charge-density wave (CDW) or stripes[39,40]. In YBCO, CDW was observed by x-ray scattering experiments and found to reside inside the pseudogap phase and competes with superconductivity[2–5]. CDW was also found in Bi2212 and to compete with superconductivity[41,42] as in the case of YBCO. More recent work on underdoped Bi2212 ($T_c = 40$ K) showed that the elastic peak that represents the CDW survived up to T^*[43]. From the fact that static CDW in Bi2212 competes with superconductivity and possibly survives up to T^* including our case, it is also likely that the nematicity observed in our measurements arises from fluctuating CDW. Furthermore, there have been recent theoretical attempts to explain the nematicity on the basis of the pair-density wave (PDW) model[44,45]. As shown in the calculated single-particle spectra in ref. [45], the inequivalence between the X and Y points may be attributed of the intensity difference predicted for incommensurate PDW states at finite temperatures.

In Fe-based superconductors, nematicity has been observed as the different populations of different orbitals (such as yz vs. zx orbitals) revealed by ARPES experiments[46]. In the present study, the observed anisotropy might be due to the different populations of the oxygen p_x and p_y orbitals because the entire Fermi surface consists of the copper $3d_x2_-y2$ orbital hybridized with the oxygen p_x and p_y orbitals[47]. However, nematicity can also be triggered by other mechanisms, e.g., the Pomeranchuk instability in single band systems and, therefore, it is not clear whether the anisotropy of the orbital populations is important to explain the nematicity observed in the cuprates as in the case of the Fe-based superconductors. Although, at present it is difficult to identify the microscopic origin of the nematicity, our result provides evidence that the pseudogap state shows nematicity and competes with superconductivity. In contrast, the STM experiments have indicated nematicity even in the superconducting state[48]. In order to reconcile the STM experiments with the apparent competition between the nematicity and the superconductivity implied in the present study, there is the possibility that the nematicity is masked by the d-wave superconducting order parameter, whose amplitude should be identical between the two Cu-O bond directions, in the present ARPES data.

In conclusion, we have demonstrated the presence of nematicity in the pseudogap state of Pb-Bi2212 by temperature-dependent ARPES experiments as suggested in previous studies. On top of that, possible suppression of the nematicity in the superconducting state was also indicated. However, there are still unsolved issues regarding the pseudogap, that is, how the nematicity is related to the other observed orders inside the pseudogap phase, e.g., CDW[2–6], which induces translational symmetry breaking and loop current order[7–10,49] which induces time-reversal symmetry breaking. If a unidirectional CDW is fluctuating, translational symmetry may be recovered and result in a $Q = 0$ nematic order and a pseudogap of the CDW origin may persist in the quasiparticle band dispersion[50]. Further work is necessary to elucidate the nature and the origin of nematicity.

METHODS

Sample preparation

Pb-Bi2212 single crystals were grown by the floating-zone method. The hole concentration was slightly overdoped one ($T_c = 91$ K) after annealing the samples in a N_2 flow, which allowed us to measure samples above and below T^* (~160 K) rather easily compared to the underdoped samples whose T^*'s are too high[51]. We measured Pb-doped samples in order to suppress the superstructure modulation present in the BiO layers of Bi2212, which causes the so-called diffraction replicas of the Fermi surface shifted by multiples of $\boldsymbol{k} = \pm(0.21\pi, 0.21\pi)$[30].

YBCO has Cu–O chains in addition to the CuO_2 plane, which help nematic domains to align in one particular direction, while Pb-Bi2212 has no such an internal source of strain as the Cu–O chains and the in-plane crystal structure is tetragonal. Therefore, we applied a tensile strain to the sample along the Cu–O bond direction in attempt to align nematic domains in one direction using a device similar to that used for Fe-based superconductors, a picture and a schematic figure of which are shown in Supplementary Fig. 10c[52]. Here, in analogy to ferromagnets, the tensile strain plays a role of a weak external magnetic field that align ferromagnetic domains along the field direction[29]. The strain was applied in air at room temperature, and the stressed sample was introduced into the ultrahigh vacuum and cooled down to measurement temperatures before cleaving in situ (See Supplementary Note 8 for the strain estimated from the lattice parameters by x-ray diffraction measurement). Such an operation was necessary to obtain anisotropic signals from spectroscopic data because the size of the nematic domains is not necessarily larger than the beam size; otherwise, anisotropic signals may be averaged out[46,53]. Note that in our experimental setup, it is impossible to detect nematicity which is diagonal to the crystallographic a and b directions[19], i.e., so-called diagonal nematicity[54].

ARPES experiments

ARPES measurements were carried out at the undulator beamline BL5U of UVSOR using an MBS A-1 analyzer. The photon energy hν was fixed at 60 eV. The energy resolution was set at 30 meV. The linear polarization of the incident light was chosen perpendicular to the analyzer slit and the tilt axis parallel to the analyzer slit, which realizes the unique experimental configuration that preserves the equivalence of the a-axis and b-axis directions with respect to the light polarization $\boldsymbol{E}$ and the strain direction, as shown in the inset of Fig. 1. This setting guarantees that the anisotropy of the spectroscopic data between the a-axis and b-axis directions does not originate from the $\boldsymbol{A}\cdot\boldsymbol{p}$ term of the matrix element but from intrinsic

inequivalence in the electronic structure. The measurements were performed in the normal, pseudogap, and superconducting states in two series, that is, with increasing temperature and with decreasing temperature in order to check the reproductivity. The samples were cleaved in situ under the pressure better than 2×10^{-8} Pa.

DATA AVAILABILITY

All data needed to evaluate the conclusions in the paper are present in the paper and/or the Supplementary Materials. Additional data related to this paper may be requested from the authors.

Received: 4 June 2021; Accepted: 11 September 2021;
Published online: 07 October 2021

REFERENCES

1. Keimer, B., Kivelson, S. A., Norman, M. R., Uchida, S. & Zaanen, J. From quantum matter to high-temperature superconductivity in copper oxides. *Nature* **518**, 179–186 (2015).
2. Ghiringhelli, G. et al. Long-range incommensurate charge fluctuations in (Y,Nd) $Ba_2Cu_3O_{6+x}$. *Science* **337**, 821–825 (2012).
3. Chang, J. et al. Direct observation of competition between superconductivity and charge density wave order in $YBa_2Cu_3O_{6.67}$. *Nat. Phys.* **8**, 871–876 (2012).
4. Comin, R. et al. Broken translational and rotational symmetry via charge stripe order in underdoped $YBa_2Cu_2O_{6+y}$. *Science* **347**, 1335–1339 (2015).
5. Le Tacon, M. et al. Inelastic X-ray scattering in $YBa_2Cu_3O_{6.6}$ reveals giant phonon anomalies and elastic central peak due to charge-density-wave formation. *Nat. Phys.* **10**, 52–58 (2014).
6. Comin, R. et al. Charge order driven by Fermi-arc instability in $Bi_2Sr_{2-x}La_xCuO_{6+\delta}$. *Science* **343**, 390–392 (2014).
7. Fauque, B. et al. Magnetic order in the pseudogap phase of high-TC superconductors. *Phys. Rev. Lett.* **96**, 197001 (2006).
8. Mangin-Thro, L. et al. Characterization of the intra-unit-cell magnetic order in $Bi_2Sr_2CaCu_2O_{8+\delta}$. *Phys. Rev. B* **89**, 094523 (2014).
9. Mangin-Thro, L., Li, Y., Sidis, Y. & Bourges, P. a−b anisotropy of the intra-unit-cell magnetic order in $YBa_2Cu_3O_{6.6}$. *Phys. Rev. Lett.* **118**, 097003 (2017).
10. Varma, C. M. Pseudogap in cuprates in the loop-current ordered state. *J. Phys. Condens. Matter* **26**, 505701 (2014).
11. Ando, Y., Segawa, K., Komiya, S. & Lavrov, A. N. Electrical resistivity anisotropy from self-organized one dimensionality in high-temperature superconductors. *Phys. Rev. Lett.* **88**, 137005 (2002).
12. Hinkov, V. et al. Electronic liquid crystal state in the high-temperature superconductor $YBa_2Cu_3O_{6.45}$. *Science* **319**, 597–600 (2008).
13. Sato, Y. et al. Thermodynamic evidence for a nematic phase transition at the onset of the pseudogap in $YBa_2Cu_3O_y$. *Nat. Phys.* **13**, 1074–1078 (2017).
14. Lawler, M. J. et al. Intra-unit-cell electronic nematicity of the high-*Tc* copper-oxide pseudogap states. *Nature* **466**, 347–351 (2010).
15. Daou, R. et al. Broken rotational symmetry in the pseudogap phase of a high-*Tc* superconductor. *Nature* **463**, 519–522 (2010).
16. Kaminski, A. et al. Spontaneous breaking of time-reversal symmetry in the pseudogap state of a high-Tc superconductor. *Nature* **416**, 610–613 (2002).
17. De Almeida-Didry, S. et al. Evidence for intra-unit-cell magnetic order in $Bi_2Sr_2CaCu_2O_{8+\delta}$. *Phys. Rev. B* **86**, 020504 (2012).
18. Cyr-Choinière, O. et al. Two types of nematicity in the phase diagram of the cuprate superconductor $YBa_2Cu_3O_y$. *Phys. Rev. B* **92**, 224502 (2015).
19. Wu, J., Bollinger, A. T., He, X. & Božović, I. Spontaneous breaking of rotational symmetry in copper oxide superconductors. *Nature* **547**, 432–435 (2017).
20. Kivelson, S. A., Fradkin, E. & Emery, V. J. Electronic liquid-crystal phases of a doped Mott insulator. *Nature* **393**, 550–553 (1998).
21. Kivelson, S. A. et al. How to detect fluctuating stripes in the high-temperature superconductors. *Rev. Mod. Phys.* **75**, 1201–1241 (2003).
22. Yamase, H. & Kohno, H. Instability toward formation of quasi-one-dimensional fermi surface in two-dimensional $t - J$ model. *J. Phys. Soc. Jpn.* **69**, 2151–2157 (2000).
23. Yamase, H. & Metzner, W. Magnetic excitations and their anisotropy in $YBa_2Cu_3O_{6+x}$: slave-boson mean-field analysis of the bilayer *t-J* model. *Phys. Rev. B* **73**, 214517 (2006).
24. Oganesyan, V., Kivelson, S. A. & Fradkin, E. Quantum theory of a nematic Fermi fluid. *Phys. Rev. B* **64**, 195109 (2001).
25. Kao, Y.-J. & Kee, H.-Y. Anisotropic spin and charge excitations in superconductors: signature of electronic nematic order. *Phys. Rev. B* **72**, 024502 (2005).
26. Halboth, C. J. & Metzner, W. *d*-wave superconductivity and pomeranchuk instability in the two-dimensional hubbard model. *Phys. Rev. Lett.* **85**, 5162–5165 (2000).
27. Auvray, N. et al. Nematic fluctuations in the cuprate superconductor $Bi_2Sr_2CaCu_2O_{8+\delta}$. *Nat. Commun.* **10**, 5209 (2019).
28. Ishida, K. et al. Divergent nematic susceptibility near the pseudogap critical point in a cuprate superconductor. *J. Phys. Soc. Jpn.* **89**, 064707 (2020).
29. Vojta, M. Lattice symmetry breaking in cuprate superconductors: stripes, nematics, and superconductivity. *Adv. Phys.* **58**, 699–820 (2009).
30. Damascelli, A., Hussain, Z. & Shen, Z.-X. Angle-resolved photoemission studies of the cuprate superconductors. *Rev. Mod. Phys.* **75**, 473–541 (2003).
31. Feng, D. L. et al. Bilayer splitting in the electronic structure of heavily overdoped $Bi_2Sr_2CaCu_2O_{8+\delta}$. *Phys. Rev. Lett.* **86**, 5550–5553 (2001).
32. Kordyuk, A. A. et al. Origin of the peak-dip-hump line shape in the superconducting-state (π,0) photoemission spectra of $Bi_2Sr_2CaCu_2O_8$. *Phys. Rev. Lett.* **89**, 077003 (2002).
33. Borisenko, S. V. et al. Anomalous enhancement of the coupling to the magnetic resonance mode in underdoped Pb-Bi2212. *Phys. Rev. Lett.* **90**, 207001 (2003).
34. Kitatani, M., Tsuji, N. & Aoki, H. Interplay of Pomeranchuk instability and superconductivity in the two-dimensional repulsive Hubbard model. *Phys. Rev. B* **95**, 075109 (2017).
35. Kondo, T. et al. Anomalous asymmetry in the Fermi surface of the high-temperature superconductor $YBa_2Cu_4O_8$ revealed by angle-resolved photoemission spectroscopy. *Phys. Rev. B* **80**, 100505 (2009).
36. Okamoto, S. & Furukawa, N. Spontaneous fourfold-symmetry breaking driven by electron-lattice coupling and strong correlations in high-Tc cuprates. *Phys. Rev. B* **86**, 094522 (2012).
37. Okamoto, S., Sénéchal, D., Civelli, M. & Tremblay, A.-M. S. Dynamical electronic nematicity from Mott physics. *Phys. Rev. B* **82**, 180511 (2010).
38. Yamase, H. & Metzner, W. Competition of Fermi surface symmetry breaking and superconductivity. *Phys. Rev. B* **75**, 155117 (2007).
39. Nie, L., Tarjus, G. & Kivelson, S. A. Quenched disorder and vestigial nematicity in the pseudogap regime of the cuprates. *Proc. Natl. Acad. Sci.* **111**, 7980–7985 (2014).
40. Nie, L., Sierens, L. E. H., Melko, R. G., Sachdev, S. & Kivelson, S. A. Fluctuating orders and quenched randomness in the cuprates. *Phys. Rev. B* **92**, 174505 (2015).
41. Hashimoto, M. et al. Direct observation of bulk charge modulations in optimally doped $Bi_{1.5}Pb_{0.6}Sr_{1.54}CaCu_2O_{8+\delta}$. *Phys. Rev. B* **89**, 220511 (2014).
42. da Silva Neto, E. H. et al. Ubiquitous interplay between charge ordering and high-temperature superconductivity in cuprates. *Science* **343**, 393 (2014).
43. Chaix, L. et al. Dispersive charge density wave excitations in $Bi_2Sr_2CaCu_2O_{8+\delta}$. *Nat. Phys.* **13**, 952–956 (2017).
44. Dai, Z., Zhang, Y.-H., Senthil, T. & Lee, P. A. Pair-density waves, charge-density waves, and vortices in high-*Tc* cuprates. *Phys. Rev. B* **97**, 174511 (2018).
45. Tu, W.-L. & Lee, T.-K. Evolution of pairing orders between pseudogap and superconducting phases of cuprate superconductors. *Sci. Rep.* **9**, 1719 (2019).
46. Yi, M. et al. Symmetry-breaking orbital anisotropy observed for detwinned $Ba(Fe_{1-x}Co_x)_2As_2$ above the spin density wave transition. *Proc. Natl. Acad. Sci.* **108**, 6878–6883 (2011).
47. Yamakawa, Y. & Kontani, H. Spin-fluctuation-driven nematic charge-density wave in cuprate superconductors: impact of Aslamazov-Larkin vertex corrections. *Phys. Rev. Lett.* **114**, 257001 (2015).
48. Fujita, K. et al. Simultaneous transitions in cuprate momentum-space topology and electronic symmetry breaking. *Science* **344**, 612–616 (2014).
49. Kontani, H., Yamakawa, Y., Tazai, R. & Onari, S. Odd-parity spin-loop-current order mediated by transverse spin fluctuations in cuprates and related electron systems. *Phys. Rev. Res.* **3**, 013127 (2021).
50. Mukhopadhyay, S. et al. Evidence for a vestigial nematic state in the cuprate pseudogap phase. *Proc. Natl Acad. Sci.* **116**, 13249–13254 (2019).
51. Vishik, I. M. et al. Phase competition in trisected superconducting dome. *Proc. Natl Acad. Sci.* **109**, 18332–18337 (2012).
52. Schütt, M. & Fernandes, R. M. Antagonistic in-plane resistivity anisotropies from competing fluctuations in underdoped cuprates. *Phys. Rev. Lett.* **115**, 027005 (2015).
53. Shimojima, T. et al. Lifting of *xz/yz* orbital degeneracy at the structural transition in detwinned FeSe. *Phys. Rev. B* **90**, 121111 (2014).
54. Murayama, H. et al. Diagonal nematicity in the pseudogap phase of $HgBa_2CuO_{4+\delta}$. *Nat. Commun.* **10**, 3282 (2019).

ACKNOWLEDGEMENTS

Informative discussion with T. K. Lee, H. Yamase, T. Shibauchi, and K. Ishida is gratefully acknowledged. A part of this work was conducted at Advanced Characterization Nanotechnology Platform of the University of Tokyo, supported by"Nanotechnology Platform" of the Ministry of Education, Culture, Sports, Science and Technology (MEXT), Japan. ARPES experiments were performed at UVSOR (Proposal Nos. 28–813 and

29–821). This work was supported by KAKENHI Grant No. 15H02109, 19K03741, and JP19H05823 and by "Program for Promoting Researches on the Supercomputer Fugaku" (Basic Science for Emergence and Functionality in Quantum Matter—Innovative Strongly-Correlated Electron Science by Integration of "Fugaku" and Frontier Experiments, JPMXP1020200104) from MEXT.

AUTHOR CONTRIBUTIONS

S.N., M.H., K.K., K.H., C.L., and M.S. performed ARPES measurements with the assistance of S.I. and K.T. S.N. analyzed the data. D.S., Y.Y., and E.H. synthesized and characterized single crystals. S.N. and A.F. wrote the manuscript with suggestions by M.H., D.S., and all other coauthors. A.F. was responsible for overall project direction and planning.

COMPETING INTERESTS

The authors declare no competing interests.

ADDITIONAL INFORMATION

Supplementary information The online version contains supplementary material available at https://doi.org/10.1038/s41535-021-00390-x.

Correspondence and requests for materials should be addressed to S. Nakata.